Available online at www.sciencedirect.com
ScienceDirect
Bioorganic & Medicinal Chemistry 16 (2008) 5914–5925
Bioorganic & Medicinal Chemistry

Synthesis, nano-scale assembly, and in vivo anti-thrombotic activity of novel short peptides containing L-Arg and L-Asp or L-Glu

Yu Chen,[a] Guohui Cui,[b] Ming Zhao,[b,*] Chao Wang,[a] Keduo Qian,[c] Susan Morris-Natschke,[c] Kuo-Hsiung Lee[c,*] and Shiqi Peng[a,b,*]

[a]*College of Pharmaceutical Sciences, Peking University, Beijing 100083, PR China*
[b]*College of Pharmaceutical Sciences, Capital Medical University, Beijing 100069, PR China*
[c]*Natural Products Research Laboratories, School of Pharmacy, University of North Carolina, Chapel Hill, NC 27599, USA*

Received 16 November 2007; revised 24 April 2008; accepted 24 April 2008
Available online 29 April 2008

Abstract—Two tripeptides H-Asp(Arg)-Arg (**3a**) and H-Glu(Arg)-Arg (**3b**), four pentapeptides H-Asp(Arg-Asp)-Arg-Asp (**6a**), H-Glu(Arg-Asp)-Arg-Asp (**6b**), H-Asp(Asp- Arg)-Asp-Arg (**10a**), and H-Glu(Asp-Arg)-Asp-Arg (**10b**), and their Cu(II)–peptide complexes Cu(II)-Asp(Arg)-Arg [**3a–Cu(II)**], Cu(II)–Glu(Arg)-Arg [**3b–Cu(II)**], Cu(II)-Asp(Arg-Asp)-Arg-Asp [**6a–Cu(II)**], Cu(II)–Glu(Arg-Asp)-Arg-Asp [**6b–Cu(II)**], Cu(II)-Asp(Asp-Arg)-Asp-Arg [**10a–Cu(II)**], and Cu(II)–Glu(Asp-Arg)-Asp-Arg [**10b–Cu(II)**] were designed and synthesized. Their self-assembling properties and in vivo anti-thrombotic activities were investigated. In normal saline (NS), the Cu(II)–peptide complexes assembled into stable nano-particles surrounded by negative charges (−4.102 to −9.825 mV), with diameters ranging from 212.1 ± 4.0 to 632.4 ± 36.7 nm. TEM analysis exhibited that the compounds remained as nano-globes in the solid state, with diameters ranging from 15 to 20 nm. In an in vivo anti-thrombotic assay, peptides **(3,6,10)a,b** at 5 μmol/kg reduced the thrombus weights of a rat model by 15–40%. Aspirin, a widely used anti-thrombotic drug, achieved comparable activity in this model system at a dosage of ca. 110 μmol/kg. The required dosage of Cu(II)–peptide complexes **[(3,6,10)a,b]–Cu(II)**, which assemble into stable nano-particles, was significantly reduced to 0.05 μmol/kg. Therefore, the anti-thrombotic activity of the nano-particles **[(3,6,10)a,b]–Cu(II)** increased dramatically by 100-fold over that of the corresponding peptides.

1. Introduction

Platelet activation and aggregation are principal processes in thromboembolic disorders.[1] The formation of an occlusive thrombus in the lumen of an injured vessel depends on a successive process of activation, adherence, and aggregation of platelets.[2,3] A thrombus can result in arteriosclerosis, heart attack, stroke, and peripheral vascular disease.[4] Although thrombosis is significant in the development of cardiovascular diseases, the currently available anti-thrombotic drugs are limited, and anti-platelet drugs are only partially effective in preventing cerebrovascular thrombus formation. Thus, the discovery of novel anti-thrombotic agents has attracted much interest.[5]

Optimizing the ability of a drug to inhibit platelet activation is essential in the development of anti-thrombotic drugs.[6] The L-arginine pathway in blood vessel endothelial cells is among the numerous platelet activation pathways that have been extensively studied. It is responsible for generation of the endogenous nitrovasodilator (NO).[7] NO plays a fundamental role in keeping blood vessels in a dilated state and maintaining the surface of the endothelium nonthrombogenic.[8] By bonding the ferroheme center of the enzyme and consequently generating cGMP, NO stimulates the release of soluble guanylate cyclase,[9] and by increasing cGMP concentration, NO induces vasodilation and anti-platelet aggregation.[10] Both the vasodilation and anti-platelet properties of NO are considered as pharmacologic foundations of

Keywords: Asp-Arg-peptides; Glu-Arg-peptides; Cu(II)-complex; Synthesis; Self-assembling; Anti-thrombotic activity.
* Corresponding authors. Tel.:+86 10 82802482; fax: +86 10 82802482 (M.Z.); tel.: +1 919 962 0066; fax: +1 919 966 3893 (K.-H.L.); tel.: +86 10 83911528; fax: +86 10 83911528 (S.P.); e-mail addresses: khlee@unc.edu; sqpeng@email.bjmu.edu.cn

0968-0896/$ - see front matter © 2008 Elsevier Ltd. All rights reserved.
doi:10.1016/j.bmc.2008.04.064

nitrovasodilators.[11] Thus, it is well established that L-arginine pathway modulators, such as NO donors and L-arginine, are beneficial in thromboembolic complications.[12]

In our previous study, a polymer containing L-arginine and L-aspartic acid was prepared as an anti-platelet aggregation peptide (PDR).[13,14] Although PDR (MW more than 30,000) exhibited anti-thrombotic activity in an in vivo assay, it had shortcomings that are inherent to polymers, including inexact molecule weight and uncertain proportion of L-arginine to L-aspartic acid residues. Thus, structural simplification of PDR was merited. In addition, we also explored the physicochemical properties of PDR, which exhibited low water solubility and an amphipathic tendency. Thus, we postulated that structural simplification of PDR could result in proper regulation of the amphipathic nature consistent with self-assembling property.

In this study, two tripeptides H-Asp(Arg)-Arg (**3a**) and H-Glu(Arg)-Arg (**3b**) as well as four pentapeptides H-Asp(Arg-Asp)-Arg-Asp (**6a**), H-Glu(Arg-Asp)-Arg-Asp (**6b**), H-Asp(Asp-Arg)-Asp-Arg (**10a**), and H-Glu(Asp-Arg)-Asp-Arg (**10b**) were designed and synthesized to mitigate the polymeric drawbacks of PDR, while retaining its anti-thrombotic activity. The self-assembling properties of these short peptides were investigated and their in vivo anti-thrombotic activities were evaluated in a rat model. Because peptides can have tremendous potential for self-assembly by defining secondary and tertiary structures and increasing various non-covalent interactions, they are considered to be naturally occurring self-assembling species.[15–20] Moreover, self-assembling peptides usually exhibit a tendency to form nanosystems, which can have distinctive properties.[21–24] Thus, Cu(II) complexes of the designed peptides (**3, 6,10)a,b** were also prepared in our study. The self-assembly and diameters of the complexes **[(3,6,10)a,b]–Cu(II)** were investigated in both NS solution and solid state, and compared with those of **(3,6,10)a,b**. Their in vivo anti-thrombotic activities were also evaluated in our rat model and compared with those of **(3,6,10)a,b**.

2. Results and discussion

2.1. Synthesis

The short peptides were synthesized as shown in Scheme 1. Solution methodology and stepwise synthesis from C-terminus to N-terminus were applied. In the presence of dicyclohexylcarbodiimide (DCC), separate reactions of *p*-nitrophenol with Boc-Asp-OH and Boc-Glu-OH yielded Boc-Asp(ONp)-ONp (**1a**) and Boc-Glu(ONp)-ONp (**1b**) in 83% and 84% yields, respectively. At pH 8.5–9.0, amidation of **1a** and **1b** with H-Arg provided Boc-Asp(Arg)-Arg (**2a**, 80% yield) and Boc-Glu(Arg)-Arg (**2b**, 85% yield). Removal of the Boc group converted **2a** and **2b** to **3a** (88% yield) and **3b** (78% yield). In the presence of 1-hydroxybenzotriazole (HOBt), DCC, and *N*-methylmorpholine (NMM), **2a** and **2b** were coupled with H-Asp(OMe)-OMe to give Boc-Asp[Arg-Asp(OMe)-OMe]-Arg-Asp(OMe)-OMe (**4a**, 58% yield) and Boc-Glu[Arg-Asp(OMe)-OMe]-Arg-Asp(OMe)-OMe (**4b**, 65% yield), respectively. Saponification of **4a** and **4b** provided Boc-Asp(Arg-Asp)-Arg-Asp (**5a**) and Boc-Glu(Arg-Asp)-Arg-Asp (**5b**) in 75%

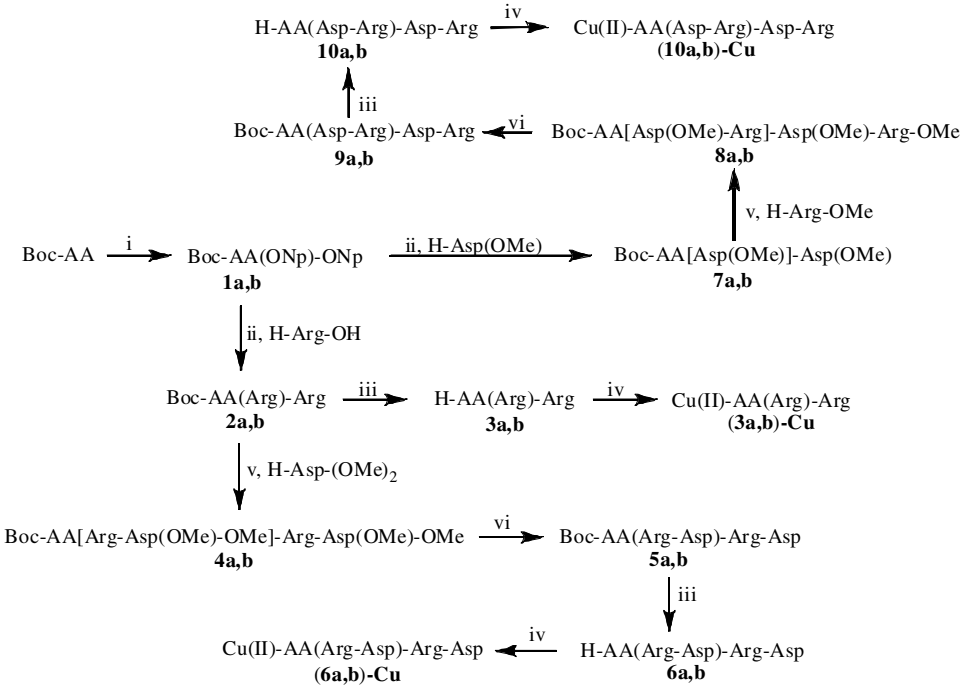

Scheme 1. Synthetic route of **(3,6,10)a,b** and **[(3,6,10)a,b]–Cu(II)**. In **1a–10a** AA = L-Asp, in **1b–10b** AA = L-Glu. Reagents: (i) DCC, HONp anhydrous THF and Boc-Asp-OH or Boc-Glu-OH; (ii) $NaHCO_3$ and NMM; (iii) CF_3CO_2H; (iv) $CuCl_2{\cdot}H_2O$ and Na_2CO_3; (v) HOBt, DCC and NMM; (vi) NaOH and $KHSO_4$.

and 68% yields, respectively. Treating **5a** and **5b** with trifluoroacetic acid (TFA) removed the Boc group and generated **6a** (63% yield) and **6b** (69% yield). Similarly, by using H-Asp(OMe) rather than H-Arg, amidation of **1a** and **1b** gave Boc-Asp[Asp(OMe)]-Asp(OMe) (**7a**, 81% yield) and Boc-Glu[Asp(OMe)]-Asp(OMe) (**7b**, 67% yield), respectively. The same reaction sequences described above were used to synthesize Boc-Asp[Asp(OMe)-Arg-OMe]-Asp(OMe)-Arg-OMe (**8a**, 80% yield) and Boc-Glu-[Asp(OMe)-Arg-OMe]-Asp(OMe)-Arg-OMe (**8b**, 70% yield), followed by Boc-Asp(Asp-Arg)-Asp-Arg (**9a**, 75% yield) and Boc-Glu-(Asp-Arg)-Asp-Arg (**9b**, 90% yield), and finally **10a** (75% yield) and **10b** (86% yield). At pH 8, reaction of (**3, 6, 10**)**a,b** with $CuCl_2$ provided Cu(II)–peptide complexes **3a**–**Cu(II)**, **3b**–**Cu(II)**, **6a**–**Cu(II)**, **6b**–**Cu(II)**, **10a**–**Cu(II)** and **10b**–**Cu(II)** in 58%, 78%, 63%, 69%, 75% and 90% yields, respectively (Scheme 1).

2.2. Nano-scale assembling of (3,6,10)a,b in NS

Nano-scale assembling of (**3,6,10**)**a,b** in NS solution was analyzed using a Malvern's Zeta Sizer (Nano-ZS90) with DTS (Nano) Program. However, (**3,6,10**)**a,b** were only able to self-assemble to unstable nano-particles in NS. On Day 1, the diameters of the nano-particles ranged from 473.9 ± 50.5 to 983.2 ± 48.9 nm, while on Day 2, diameters increased to 666.1 ± 23.3 to 1443.8 ± 49.7 nm. These diameters are indicative of unstable nano-particles. On Day 3, no nano-particles were detected in the NS solutions. The recorded diameters are shown in Figure 1.

2.3. Nano-scale assembling of [(3,6,10)a,b]–Cu(II) complexes in NS

As previously mentioned, peptides can have tremendous potential for self-assembly through increased non-covalent interactions, and can form nanosystems with distinctive properties. To increase the potential for our newly synthesized peptides to form stable nano-particles, we selected Cu(II) as a complexing metal ion. Since the d–d transition in UV–vis and CD spectra is generally used to identify Cu(II) coordination, the UV–vis and CD spectra of the free peptides (**3,6,10**)**a,b** and their Cu(II) complexes [(**3,6,10**)**a,b**]–**Cu(II)** were measured and are shown in Figures 2 and 3.

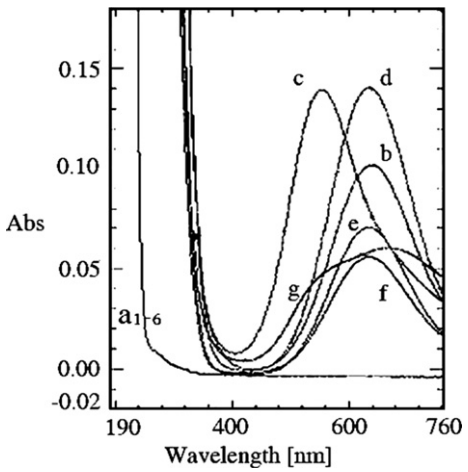

Figure 2. UV spectra of aqueous solutions of (**3,6,10**)**a,b** and [(**3,6,10**)**a,b**]–**Cu(II)**. Maximum absorbance over 560–660 nm relates to the d–d transition of Cu(II)–peptide complexes. Temperature 25 °C; concentration 1 mM; a_1, a_2, a_3, a_4, a_5 and a_6 represent **10b, 10a, 6b, 6b, 6a, 3b** and **3a**, respectively; b, c, d, e, f and g represent **10b**–**Cu(II)**, **10a**–**Cu(II)**, **6b**–**Cu(II)**, **6a**–**Cu(II)**, **3b**–**Cu(II)** and **3a**–**Cu(II)**, respectively.

Except for caudal absorbance from 190 to 240 nm, the free peptides (**3,6,10**)**a,b** displayed no UV absorbance at any other wavelength. After Cu(II) complexation, the spectra changed dramatically and strong bands were observed in the region from 560 to 660 nm for all six complexes. These significant spectral changes, attributed to Cu (II) d–d transition, indicate changes in the environment of the carbonyl group in the peptide bond and possible coordination of the peptide bonds with the metal cation.[25] A similar absorbance was also reported to occur in a related Cu(II)-coordinated nanostructure.[26]

The CD spectra of the free peptides (**3,6,10**)**a,b** and their Cu(II) complexes [(**3,6,10**)**a,b**]–**Cu(II)** confirmed the UV results and conclusions. The free peptides had positive Cotton effects from 217 to 225 nm, suggesting they had unordered structures. Stereoviews of the free peptides' lowest energy conformations were drawn using Discovery Studio Program (Fig. 4). These conformations showed that the free peptides' carbonyl groups were exposed and unable to take part in repetitive H bonds. On the other hand, in the spectral region from 600 to 660 nm,

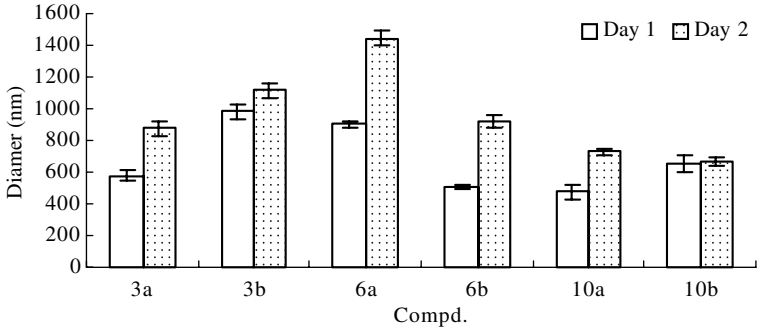

Figure 1. Particle diameters of (**3**,**6**,**10**)**a**,**b** assembled in NS. Test temperature was 25 °C, solution concentration of (**3,6,10**)**a,b** in NS was 1 mg/mL, particle diameter is expressed by $\overline{X} \pm$ SD nm, $n = 10$.

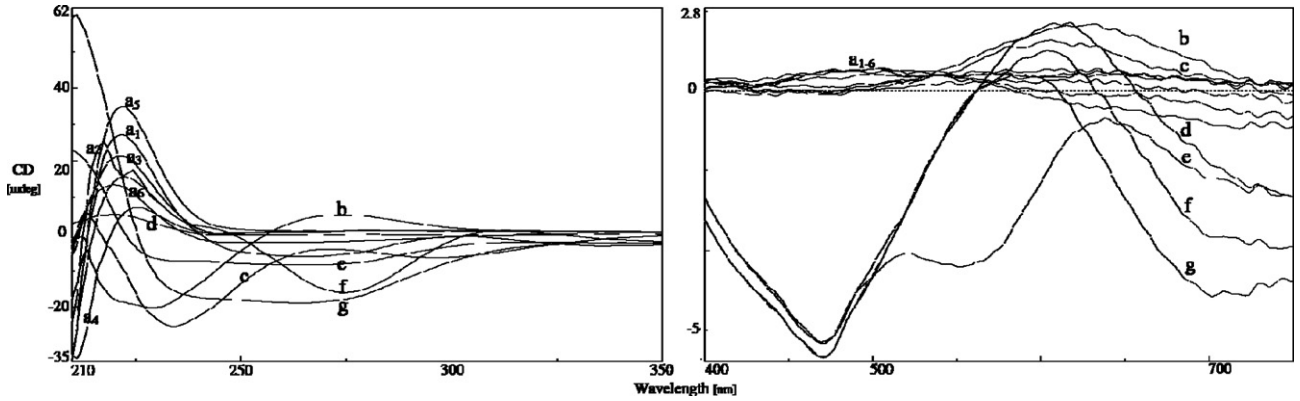

Figure 3. CD spectra of **(3,6,10)a,b** and **[(3,6,10)a,b]–Cu(II)** in water. CD spectra of **[(3,6,10)a,b]–Cu(II)** displayed an absorbance around 600–660 nm, which is considered to result from the d–d transition of Cu(II) coordination. Temperature 25 °C; concentration 1 mM; a_1, a_2, a_3, a_4, a_5 and a_6 represent **10b, 10a, 6b, 6b, 6a 3b** and **3a**, respectively; b, c, d, e, f and g represent **10b–Cu(II)**, **10a–Cu(II)**, **6b–Cu(II)**, **6a–Cu(II)**, **3b–Cu(II)** and **3a–Cu(II)**, respectively.

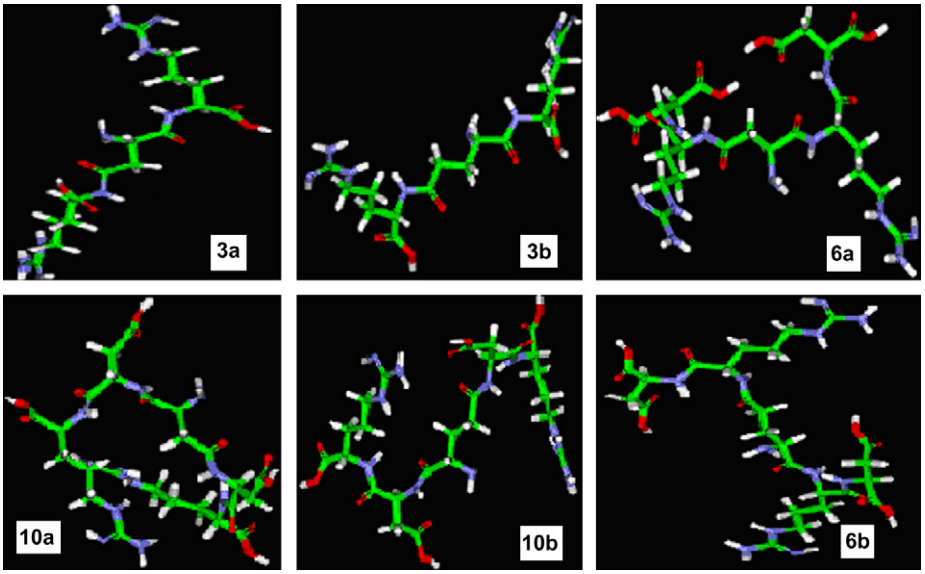

Figure 4. Discovery Studio Program drawing lowest energy conformations of **(3,6,10)a,b**.

the free peptides displayed no absorbance, while their Cu(II) complexes did, which is likely a result of the d–d transition of Cu(II) coordination.[27]

A nano-particle size analysis of **[(3,6,10)a,b]–Cu(II)** complexes in NS demonstrated that these complexes did assemble more easily into stable nano-particles compared with **(3,6,10)a, b** (Fig. 1). On Day 1, the diameters of the nano-particles ranged from 212.1 ± 4.0 to 632.4 ± 36.7 nm, on Day 4, the diameter size increased to 382.4 ± 16.0 to 755.0 ± 204.4 nm, and on Day 7, the nano-particles were still stable with detectable diameters. The recorded diameters over 4 days are shown in Figure 5.

To gain insights into the relationship between nano-particle stability and peptide structure, the diameter changes were compared. For this purpose, the particle diameter of the assembled Cu(II) complexes on Day 1 was taken as the norm, the diameters of Days 2–4 were averaged, and the difference between the average and norm values was used to represent the diameter change. The data are listed in Table 1.

Comparison of the diameter change demonstrated the following facts. The diameter increase of **[(3,6)b]–Cu(II)**, which have Glu as the central linker, was less than that of **[(3,6)a]–Cu(II)**, with Asp as the central linker, (2.2% and 20.6% versus 58.4% and 102%, respectively). Correspondingly, the diameter decrease of **10b–Cu(II)**, central residue is Glu, was more than that of **10a–Cu(II)**, central residue is Asp, (27.1% vs 0.5%). These results indicate that the former Glu-linked complexes were more stable as nano-particles than the latter Asp-linked complexes. In the calculated lowest conformations, the distances between the guanidiniums in peptides with a Glu residue as the central linker are larger than those of the peptides with an Asp residue as the central linker, which implies that the former are more flexible and may limit particle growth.

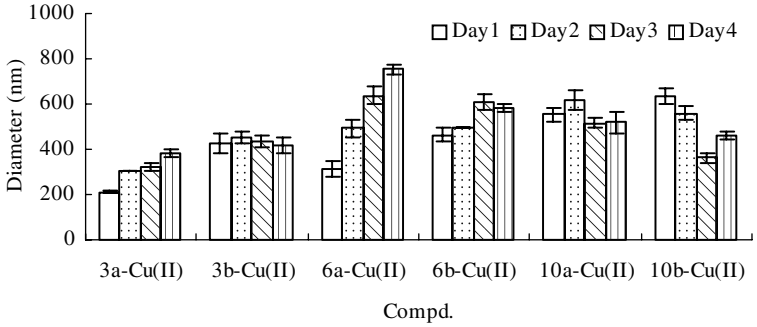

Figure 5. Particle diameters of **[(3,6,10)a,b]–Cu(II)** assembled in NS. Test temperature was 25 °C, solution concentration of **[(3,6,10)a,b]–Cu(II)** in NS was 1 mg/mL, diameter is expressed by $\overline{X} \pm$ SD nm, and on the 7th day the nano-systems were still stable, $n = 10$.

2.4. Zeta-potentials of (3,6,10)a,b and [(3,6,10)a,b]–Cu(II) nano-particles in NS

To examine the electrical stabilities of (**3**,**6**,10) **a,b** and **[(3,6,10)a,b]–Cu(II)** nano-particles in solution state, the Zeta potentials in NS were measured. Table 2 lists the Zeta potentials on the nano-particle surfaces of **(3,6,10) a,b** at Hour 1 and of **[(3,6,10) a,b]–Cu(II)** on Day 4 after their preparation in NS solution.

The results indicated that, except for **10b**, the surfaces of **(3, 6)a,b** and **10a** nano-particles were surrounded by negative charges. It is reasonable to propose that the self-assembly of **(3, 6)a,b** and **10a** in NS is driven by hydrophobic interactions between residues and results in hydrophilic guanidiniums being exposed. The conformational stereoviews (Fig. 4) of **(3,6)a,b** and **10a** support such an arrangement of the protonated guanidiniums. Therefore, the nano-particles' surfaces will be positively charged and surrounded by negative charges. However, looking at the stereoview of **10b**, controlled self-assembly could instead expose negative charges. Therefore, its nano-particles' surface would be negatively, rather than positively, charged and surrounded by positive charges. The surfaces of **[(3,6)a,b,10a]–Cu(II)** nano-particles were also surrounded by negative charges, demonstrating that, even after **Cu(II)** complexation, the hydrophilic guanidiniums remained exposed. In addition, **Cu(II)** complexation of **10b** apparently led to a changed mode of self-assembly and consequently to exposed hydrophilic guanidiniums.

Surface zeta potential is generally considered as a measurement of the charge density per unit surface, which depends on both the total of charged groups and the size of the nano-particle. Although **3a** and **3b** have equal numbers of protonated guanidiniums, the particle size of the former is significantly smaller than that of the latter; thus, the zeta potential of the former is significantly higher than that of the latter. In contrast, although the particle size of **6a** is significantly smaller than that of **6b**, the two compounds have comparable zeta potentials. An explanation is found from the stereoviews of the lowest energy conformations shown in Figure 4. When **6a** assembles, two guanidiniums will likely be exposed; however, when **6b** assembles, only one guanidinium will be exposed. These opposing effects (size and total charge) lead to the two compounds having equal zeta potentials. Similarly, although **10a** is smaller than **10b**, each exposed guanidinium of **10a** has at least two protonated nitrogens, while each exposed carboxyl can ionize giving only one acid group. Therefore the absolute Zeta potential of **10a** is significantly higher than that of **10b**.

Table 2 also indicates, except for **3b** and **10b**, the Zeta potentials of the remaining peptides (**3a**, **6a, 6b**, and **10a**) at Hour 1 generally were equal to those of their cor-

Table 1. Dependence of particle diameter on peptide–Cu(II) structure

Compound	Diameter			
	Central residue	Day 1	Mean of Days 2-4	Increase in respect to Day 1 (%)
3a–Cu(II)	Asp	212.1	335.9	58.4
3b–Cu(II)	Glu	424.4	433.8	2.2
6a–Cu(II)	Asp	311.6	629.4	102
6b–Cu(II)	Glu	465.1	560.8	20.6
10a–Cu(II)	Asp	553.1	550.3	−0.5
10b–Cu(II)	Glu	632.4	459.9	−27.3

Table 2. Zeta potential and size of **(3,6,10)a,b** and **[(3,6,10)a,b]–Cu(II)** nano-particles

Compound	Hour 1		Compound	Day 4	
	Zeta potential	Diameter		Zeta potential	Diameter
3a	−6.405	304.9 ± 10.3	**3a–Cu(II)**	−6.284	382.4 ± 16.0
3b	−1.901	431.4 ± 32.1	**3b–Cu(II)**	−6.472	416.0 ± 33.1
6a	−5.578	749.8 ± 17.8	**6a–Cu(II)**	−5.262	755.0 ± 20.4
6b	−4.592	536.4 ± 21.1	**6b–Cu(II)**	−4.102	579.6 ± 17.8
10a	−9.159	550.8 ± 27.2	**10a–Cu(II)**	−9.825	518.3 ± 50.2
10b	2.101	503.5 ± 16.5	**10b–Cu(II)**	−8.959	460.1 ± 15.7

responding **Cu(II)** complexes on Day 4. This observation is consistent with the requirement that zeta potential depends on the particle size, as the nano-particle diameters at Hour 1 and on Day 4 were also close as shown in Table 2. However, the particle size of **3b** was significantly larger than that of its **Cu(II)** complex and consequently the Zeta potential of **3b** was significantly lower than that of its **Cu(II)** complex. The distinct Zeta potentials for **10b** and **10b–Cu(II)** should be the result of their separate assembly models, as discussed above.

2.5. Nano-particle powders of (3,6,10)a,b and [(3,6,10)a,b]–Cu(II)

Generally nano-solutions can be converted into nano-solids. To confirm this possibility with our compounds, solutions (1 mg/mL) of (**3, 6,10**) **a,b** and [(**3,6,10**) **a,b**]–**Cu(II)** in triple-distilled water were evaporated at room temperature to form powders. The particle sizes of the powders were analyzed by using transmission electron microscopy (TEM). The obtained TEM photographs of (**3,6,10**)**a,b** and [(**3,6,10**)**a,b**]–**Cu(II)** powders showed that they were present as nano-globes in the solid state, and their diameters ranged from 15 to 30 nm. Representative photographs of **3a**, **10a**, **3a–Cu(II)**, **3b–Cu(II)**, **10a–Cu(II)**, and **10b–Cu(II)** powders are shown in Figure 6. The particle sizes shown in the photographs indicate that both peptides (**3,6,10**)**a,b** and the complexes [(**3,6,10**)**a,b**]–**Cu(II)** are stable nano-globes in the solid state.

2.6. In vivo anti-thrombotic activity of intravenously injected (3,6,10)a,b and [(3,6,10)a,b]-Cu(II) in NS

The in vivo anti-thrombotic activities of **3a, 3b, 6a, 6b**, **10a**, and **10b** at a dose of 5 μmol/kg and the corresponding Cu complexes at 0.05 μmol/kg in NS were assayed in our rat model. The thrombus weight was used as the measure of activity. The data indicated that the thrombus weights of rats receiving only NS (negative control) averaged 29.44 ± 5.35 mg. Intravenous dosing with (**3,6,10**)**a,b** at 5 μmol/kg reduced thrombus weights significantly by 15–40%, with weights ranging from 17.51 ± 3.71 to 25.12 ± 3.52 mg. Dosage with 110 μmol/kg of aspirin, a current widely used anti-thrombotic agent, was needed to achieve similar anti-thrombotic activity. These results suggested that our novel, designed tripeptides and pentapeptides are active against thrombosis (Fig. 7).

Because the peptides do not assemble to stable nano-particles, while the [(**3,6,10**) **a,b**]–**Cu(II)** complexes do form stable nano-systems, the anti-thrombotic activities of the nano-particle solutions of [(**3,6,10**) **a,b**]–**Cu(II)** complexes were also tested using the same general procedure. Only 0.05 μmol/kg of [(**3,6,10**) **a,b**]–**Cu(II)** complexes were needed to achieve similar anti-thrombotic activity as 5 μmol/kg of (**3,6,10**)**a,b**. By dosing [(**3,6,10**) **a,b**]–**Cu(II)** at 0.05 μmol/kg intravenously to the rats, their thrombus weights reduced significantly by 21–31%, with thrombus weights ranging from 20.31 ± 3.79 to 23.27 ± 3.32 mg. The results indicated that the formation of stable nano-particles increased the anti-thrombotic activity of the newly designed peptides by 100-fold (Fig. 7).

2.7. Dose-dependent activities of 6b, 10a, 10b, and 10a–Cu(II) in NS

Three peptides (**6b**, **10a**, and **10b**) and one Cu complex (**10a–Cu(II)**) were selected for a dose-dependent activity study. The evaluation was performed in a rat model

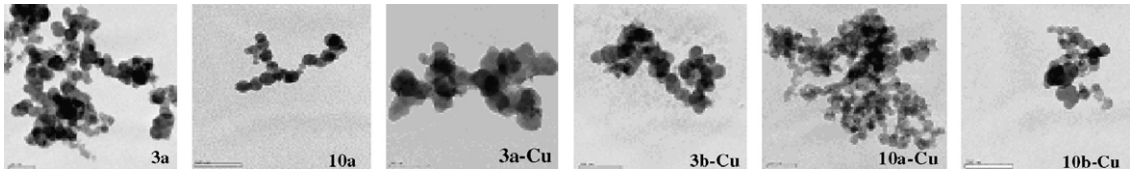

Figure 6. TEM (Model JEM-1230, JEOL, Japan) photographs of **3a**, **10a**, **3a–Cu(II)**, **3b–Cu(II)**, **10a–Cu (II)** and **10b–Cu(II)** powders.

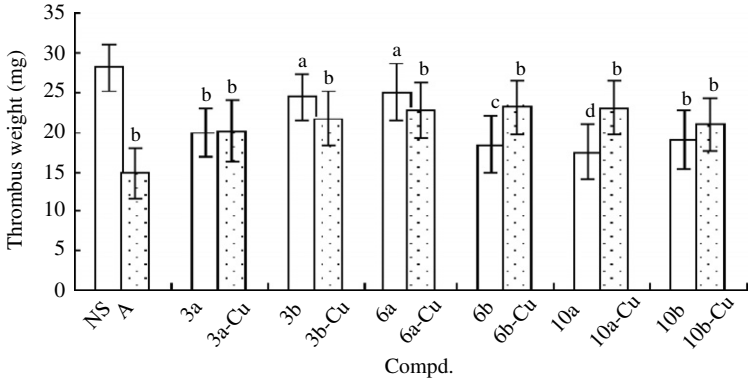

Figure 7. Thrombus weights of (**3,6,10**)**a,b** or [(**3,6,10**)**a,b**]–**Cu(II)** treated rats. NS, vehicle, $n = 12$; A, Aspirin; (**3,6,10**)**a,b**/dose = 5 μmol/kg, [(**3,6,10**) **a,b**]–**Cu(II)**/dose = 0.05 μmol/kg, Aspirin/dose = 20 mg/kg. (a) Compared to NS $p < 0.05$; (b) Compared to NS $p < 0.01$; (c) Compared to NS and **6b–Cu(II)** $p < 0.01$; (d) Compared to NS and **10a–Cu(II)** $p < 0.01$.

according to standard procedures. The data obtained indicated significant differences in the in vivo anti-thrombotic activities of the intravenously injected peptides at concentrations of 5, 0.5, 0.05, and 0.005 μmol/kg, as well as for intravenously dosed **10a–Cu(II)** at 0.5, 0.05, 0.005, and 0.0005 μmol/kg. These observations indicated that the in vivo anti-thrombotic activities of **6b**, **10a, 10b**, and **10a–Cu(II)** in NS are dose-dependent (Fig. 8).

2.8. In vivo activities of orally administrated 10a (5 μmol/kg) and 10a–Cu(II) (0.05 μmol/kg) in NS

Compounds **10a** and **10a–Cu(II)** were selected to test their oral administration profiles. The oral and intravenous data are listed in Table 3. The data indicated that orally administered **10a** (5 μmol/kg) can effectively block the thrombosis process (thrombus weight 23.18 ± 3.75 mg; compared to that of NS receiving rats, 29.44 ± 5.35 mg, $p < 0.01$). Orally dosed **10a–Cu(II)** complexes (0.05 μmol/kg) also effectively blocked the thrombosis process (thrombus weight 25.22 ± 3.79 mg; $p < 0.05$). Comparable thrombus weights were found after oral and intravenous dosing of **10a–Cu(II)**. These results suggested that both **10a** and its Cu complex [**10a–Cu(II)**] can be sufficiently absorbed in the stomach or intestine and can be administrated orally.

2.9. Correlation of the activity and nano-particle size of (3,6,10)a,b and [(3,6,10)a,b]–Cu(II)

To evaluate a possible relationship between nano-particle size and in vivo anti-thrombotic activity, the thrombus weights of rats receiving 5 μmol/kg (**3,6,10**)**a,b** or 0.05 μmol/kg [(**3,6,10**)**a,b**]–**Cu(II)** and the corresponding nano-particle diameters were compared in Table 4. Generally, a decrease in the nano-particle diameter led to an increase in the anti-thrombotic activity of (**3,6,10**)**a,b** and [(**3,6,10**)**a,b**]–**Cu(II)** complexes.

Table 3. Effect of oral administration of **10a** and **10a–Cu(II)** on thrombus weight[a]

Compound	Thrombus weight	Compound	Thrombus weight
NS (oral)	29.44 ± 3.35	Aspirin (iv)	8.50 ± 0.70[b]
10a(oral)	23.18 ± 3.75[b]	**10a** (iv)	17.506 ± 3.52[b]
10a–Cu(II) (oral)	25.22 ± 3.79[c]	**10a–Cu(II)** (iv)	23.19 ± 3.71[b]

[a] Thrombus weight is expressed by $\overline{X} \pm$ SD mg, dose of **10a** = 5 μmol/kg and of **10a–Cu(II)** = 50 nmol/kg and of Aspirin = 20 mg/kg; NS,vehicle; $n = 12$.
[b] Compare to NS $p < 0.01$.
[c] Compare to NS $p < 0.05$.

3. Conclusions

In conclusion, we designed and synthesize novel tripeptides and pentapeptides containing L-arginine and L-aspartic acid or L-glutamic acid in order to increase the anti-thrombotic activity of polyaspartyl-L-arginine (PDR), as well as alleviate its polymer shortcomings. When the residue proportions of L-arginine to L-aspartic acid or L-glutamic acid are less than 60% or more than 40%, the peptides may self-assemble. To form stable nano-particles in NS solution, Cu(II) complexes of the new peptides (**3,6,10**) **a,b** were prepared, and their nano-particle properties were measured. The in vivo anti-thrombotic activities of both (**3,6,10**) **a,b** and the Cu(II)–peptide complexes [(**3,6,10**) **a,b**]–**Cu(II)** were tested. Five micromoles per kilograms dose of (**3,6,10**) **a,b** resulted in similar anti-thrombotic activity as 110 μmol/kg of aspirin. By assembling into stable nano-particles, [(**3,6,10**)**a,b**]-**Cu(II)** complexes were 100-fold more potent than (**3,6,10**)**a,b** against thrombosis, with comparable activity at the 0.05 μmol/kg level. Potency was retained when the administration method was changed from intravenous to oral, which should facilitate potential clinical application.

4. Experimental

4.1. General procedures

Amino acids with L-configuration used were purchased from Sigma Chemical Co. Chromatography was performed on Qingdao silica gel H. The purity of intermediates and products was confirmed by TLC (Merck silica gel plates of type 60 F_{254}, 0.25 mm layer thickness) IR spectroscopy was performed on a 330 FT-IR spectrometer (Nicolet Avatar Thermo Electron Corporation). NMR spectroscopy was determined on 500 and 300 MHz spectrometers (AVANCE II, BRUKER

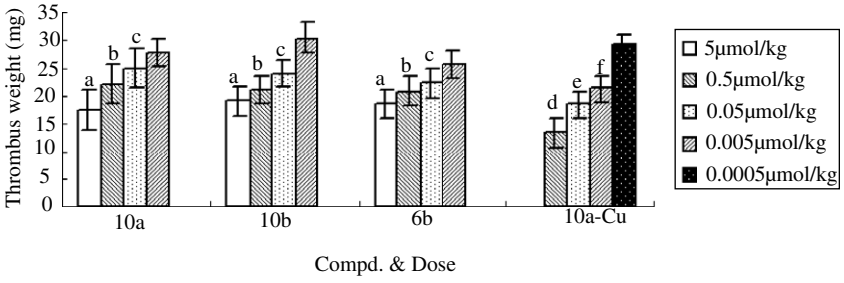

Figure 8. Dose-dependent action of **6a**, **b** and **10a** and **10a–Cu**. NS, vehicle, $n = 10$; (a) compare to NS $p < 0.001$, to 0.5 μmol/kg group $p < 0.01$; (b) compare to NS $p < 0.001$, to 0.05 μmol/kg group $p < 0.05$; (c) compare to NS $p < 0.01$, to 0.005 μmol/kg group $p < 0.05$; (d) compare to NS $p < 0.001$, to 0.05 μmol/kg group $p < 0.01$; (e) compare to NS $p < 0.01$, to 0.005 μmol/kg group $p < 0.01$; (f) compare to NS $p < 0.01$, to 0.0005 μmol/kg group $p < 0.01$.

Table 4. Interrelation of thrombus weight and particle size

Compound	Thrombus weight	Nano-particle diameter on Day 1	Compound	Thrombus weight	Nano-particle diameter on Day 4
3a	20.03 ± 3.07[c]	575.3 ± 32.9[e]	**3a–Cu(II)**	20.31 ± 3.79	382.4 ± 16.0[g]
3b	24.59 ± 2.89	983.2 ± 48.9	**3b–Cu(II)**	21.90 ± 3.31	416.0 ± 33.1[h]
6a	25.12 ± 3.52	904.0 ± 20.9	**6a–Cu(II)**	22.86 ± 3.43	755.0 ± 20.4
6b	18.68 ± 3.61[c]	507.7 ± 12.8[d]	**6b–Cu(II)**	23.27 ± 3.32	579.6 ± 17.8[k]
10a	17.51 ± 3.71[b]	473.9 ± 50.5[d]	**10a-Cu(II)**	23.19 ± 3.71	518.3 ± 50.2[j]
10b	19.19 ± 3.61[c]	653.0 ± 52.0[f]	**10b–Cu(II)**	21.14 ± 3.33[b]	460.1 ± 15.7[i]

[a]Thrombus weight is expressed by $\overline{X} \pm$ SD mg and $n = 12$, diameter is expressed by $\overline{X} \pm$ SD nm and $n = 6$; **(3,6,10)a,b**/Dose = 5 μmol/kg, [**(3,6,10)a,b**]–**Cu(II)**/Dose = 50 nmol/kg.
[b] Compare to **3b** and **6a** $p < 0.001$.
[c] Compare to **3b** and **6a** $p < 0.01$.
[d] Compare to **3a** $p < 0.05$, to **3b**, **6a** and **10b** $p < 0.001$.
[e] Compare to **10b** $p < 0.01$, to **3b** and **6a** $p < 0.001$.
[f] Compare to **3b** and **6a** $p < 0.01$.
[g] Compare to **3b** $p < 0.05$, to **6a, 6b, 10a**, and **10b** $p < 0.001$.
[h] Compare to **10b** $p < 0.05$, to **6a, 6b**, and **10a** $p < 0.001$.
[i] Compare to **10a** $p < 0.05$, to **6a, b** $p < 0.001$.
[j] Compare to **6b** $p < 0.05$, to **6a** $p < 0.001$.
[k] Compare to **6a** $p < 0.001$.

UltraShiel). ESI-MS spectroscopy was obtained with a Waters HPLC/MS (Quattro micro™ API). Optical rotations were measured on a P-1020 Jasco polarimeter (Japan).

4.2. Compounds

4.2.1. Boc-Asp(ONp)-ONP (1a). At 0 °C, 7.82 g (0.038 mol) of dicyclohexylcarbodiimide (DCC) were added portionwise to a solution of 4.36 g (0.019 mol) of Boc-Asp-OH and 5.28 g (0.038 mol) of p-nitrophenol (HONp) in 50 mL of anhydrous tetrahydrofuran (THF). The reaction mixture was stirred at 0 °C for 30 min, and then at room temperature for 12 h until TLC ($CHCl_3$/MeOH, 10:1) indicated the complete disappearance of Boc-Asp-OH. The precipitated dicylohexylcarbourea (DCU) was removed by filtration and the filtrate was evaporated under reduced pressure. The residue was crystallized from the mixture of EtOAc and petroleum ether to provide 7.5 g (83%) of the title compound.

4.2.2. Boc-Asp(Arg)-Arg (2a). A solution of 1.85 g (8.82 mmol) of HCl·H-Arg-OH and 1.48 g (17.6 mmol) of $NaHCO_3$ in 25 mL of distilled water was stirred at room temperature, and then a solution of 2.0 g (4.2 mmol) of **1a** in 5 mL of dioxane was added portionwise. The suspension was stirred and maintained at pH 8.5–9.0 by adding *N*-methylmorpholine (NMM), during which **1a** gradually dissolved and TLC ($CHCl_3$/MeOH, 20:1) indicated complete disappearance of **1a**. The reaction mixture was evaporated under reduced pressure. The residue was dissolved in 30 mL of distilled water, and the solution was extracted with diethyl ether (3× 30 mL). The aqueous phase was acidified with a saturated aqueous solution of $KHSO_4$ to pH 2 and extracted with EtOAc (3× 30 mL). The aqueous phase was evaporated under reduced pressure and the residue was dissolved in 10 mL of anhydrous EtOH. After filtration and evaporation under reduced pressure, the residue was chromatographed ($CHCl_3$/MeOH, 1:1) to give 1.83 g (80%) of the title compound. Mp 160–162 °C; ^{1}H NMR (BHSC-500, D_2O) δ 4.36 (t, $J = 5.0$ Hz, 1H), 4.18 (dd, $J = 5.0$, 8.5 Hz, 2H), 3.10 (dd, $J = 7.0$, 14.0 Hz, 4H), 2.68 (dd, $J = 9.5$, 16.0 Hz, 2H), 1.79 (m, 4H), 1.64 (m, 4H), 1.32 (s, 9H); ESI-MS (*m*/*z*) 546 $[M+H]^+$; $[\alpha]_D^{20} - 15.5$ (*c* 0.01, H_2O). Anal. Calcd for $C_{21}H_{39}N_9O_8$: C 46.23, H 7.20, N 23.11; found: C 46.40, H 7.05, N 23.30.

4.2.3. H-Asp(Arg)-Arg (3a). A solution of 500 mg (0.92 mmol) of **2a**, 1 mL of TFA, and 3 mL of CH_2Cl_2 was stirred at 0 °C for 1 h. Upon removal of TFA and CH_2Cl_2 in vacuum, the residue was triturated with diethyl ether, and the obtained powder was purified on a C18 column (CH_3CN/1% HOAc, 2.5:100) to provide 351 mg (86%) of the title compound as a colorless powder. Mp 141–145 °C; ^{1}H NMR (BHSC-500, D_2O) δ 4.23 (t, $J = 5.0$ Hz, 1H), 4.07 (dd, $J = 5.0$, 8.0 Hz, 1H), 4.03 (dd, $J = 5.0$, 8.5 Hz, 1H), 3.09 (dd, $J = 7.0$, 14.0 Hz, 4H), 2.91 (dd, $J = 5.0$, 16.0 Hz, 1H), 2.82 (dd, $J = 6.5$, 16.0 Hz, 1H), 1.73 (m, 4H), 1.48 (m, $J = 7.5$ Hz, 4H); ESI-MS (*m*/*z*) 446 $[M+H]^+$; $[\alpha]_D^{20} - 16.6$ (*c* 0.01, H_2O). Anal. Calcd for $C_{16}H_{31}N_9O_6$: C 43.14, H 7.01, N 28.30; found: C 43.00, H 7.14, N 28.11.

4.2.4. Cu(II)-Asp(Arg)-Arg [3a–Cu(II)]. To a solution of 100 mg (0.225 mmol) of **3a** in 2 mL of distilled water, 37.0 mg (0.220 mmol) of $CuCl_2 \cdot H_2O$ was added. The solution was adjusted to pH 8 with an aqueous solution of Na_2CO_3 (1 mol/L) and stirred at room temperature for 4 h. After filtration, the filtrate was evaporated under reduced pressure and the residue was purified on a Sephadex G10 column to provided 66 mg (58%) of the title compound as blue powder. IR (KBr) 3342, 2966, 2360, 1589, 1409, 1180, 699 cm^{-1}; ESI-MS (*m*/*z*) 507 $[M-1]^+$; $[\alpha]_D^{20}$62.5 (*c* 0.01, H_2O). Anal. Calcd for $C_{16}H_{30}CuN_9O_6 \cdot 2H_2O$: C 35.32, H 6.30, N 23.17; found: C 35.50, H 6.17, N 23.36.

4.2.5. Boc-Asp[Arg-Asp(OMe)-OMe]-Arg-Asp(OMe)-OMe (4a). At 0 °C, 0.238 g (1.76 mmol) of HOBt and 0.363 g (1.76 mmol) of DCC were added to a solution of 0.458 g (0.84 mmol) of **2a** in 5 mL of anhydrous

DMF. The reaction mixture was stirred at 0 °C for 10 min and then 0.346 g (1.76 mmol) of HCl·H-Asp(OMe)-OMe in 5 mL of anhydrous THF was added. The reaction mixture was adjusted to pH 8–9 with NMM, and stirred at 0 °C for 3 h and at room temperature for 12 h. The precipitated DCU was removed by filtration and the filtrate was evaporated under reduced pressure. The residue was dissolved in 10 mL of distilled water and the solution was extracted with EtOAc (3× 30 mL). The aqueous phase was acidified with saturated aqueous $KHSO_4$ to pH 2 and extracted with EtOAc (3× 30 mL). The aqueous phase was evaporated under reduced pressure and the residue was dissolved in 10 mL of anhydrous EtOH. After filtration and evaporation under reduced pressure, the residue was chromatographed ($CHCl_3$/MeOH, 10:1) to give 0.558 g (80%) of the title compound. Mp 99–100 °C; ^{1}H NMR (BHSC-300, D_2O) δ 4.26 (t, J = 5.2 Hz, 2H), 4.06 (t, J = 7.35 Hz, 2H), 3.79 (t, J = 5.2 Hz, 1H), 3.67 (d, J = 7.35 Hz, 12H), 3.15 (t, J = 6.9 Hz, 4H), 2.91 (m, 3H), 2.85 (m, 3H), 1.72 (m, 4H), 1.58 (m, 4H), 1.31 (s, 9H); ESI-MS (*m*/*z*) 832 $[M+H]^+$; $[\alpha]_D^{20}$ − 72.8 (*c* 0.01, CH_3OH). Anal. Calcd for $C_{33}H_{57}N_{11}O_{14}$: C 47.65, H 6.91, N 18.52; found: C 47.67, H 6.80, N 18.71.

4.2.6. Boc-Asp(Arg-Asp)-Arg-Asp (5a). A solution of 300 mg (0.361 mmol) of **4a**, 2 mL of MeOH, and 3 mL of aqueous NaOH (2 N) was stirred at 0 °C for 4 h. The reaction mixture was adjusted to pH 6 with saturated aqueous $KHSO_4$ and evaporated in vacuum. The residue was dissolved in 10 mL of MeOH. After filtration and evaporation under reduced pressure, 210 mg (75%) of the title compound was obtained as a colorless powder, which was used directly in the next reaction.

4.2.7. H-Asp(Arg-Asp)-Arg-Asp (6a). Using the same procedure as for **3a** and starting from 200 mg (0.258 mmol) of **5a**, 110 mg (63%) of the title compound was obtained. Mp 129–130 °C; IR (KBr) 3340, 2950, 2360, 1662, 1558, 1386, 1270, 750, 640 cm^{-1}; ^{1}H NMR (BHSC-300, D_2O) δ 4.52 (dd, J = 6.0, 12.3 Hz, 2 H), 4.26 (t, J = 5.7 Hz, 2H), 4.20 (t, J = 6.9 Hz, 1H), 3.09 (t, J = 6.3 Hz, 4H), 2.94 (dd, J = 5.1, 16.8 Hz, 4H), 2.86 (t, J = 6.9 Hz, 2H), 1.70 (m, 4H), 1.54 (t, J = 6.6 Hz, 4H); ESI-MS (*m*/*z*) 676 $[M+H]^+$; $[\alpha]_D^{20}$ − 9.8 (*c* 0.01, H_2O). Anal. Calcd for $C_{24}H_{41}N_{11}O_{12}$: C 42.66, H 6.12, N 22.80; found: C 42.50, H 6.00, N 22.62.

4.2.8. Cu(II)-Asp(Arg-Asp)-Arg-Asp [6a–Cu(II)]. Using the same procedure as that for **3a-Cu(II)**, starting from 100 mg (0.148 mmol) of **6a**, 35 mg (32%) of the title compound was obtained as blue powder. IR (KBr) 3347, 2968, 2358, 1575, 1403, 1123, 669 cm^{-1}; ESI-MS (*m*/*z*) 737$[M-1]^+$; $[\alpha]_D^{20}$ − 18.8 (*c* 0.01, H_2O). Anal. Calcd for $C_{24}H_{40}CuN_{11}O_{12}\cdot 2H_2O$: C 37.23, H 5.73, N 19.90; found: C 37.05, H 5.60, N 19.71.

4.2.9. Boc-Asp[Asp-(OMe)]-Asp-(OMe) (7a). A solution of 5.86 g (32.0 mmol) of HCl·H-Asp(OCH_3) and 5.37 g (64.0 mmol) of $NaHCO_3$ in 30 mL of distilled water was stirred at room temperature, and a solution of 7.23 g (15.2 mmol) of **1a** in 10 mL of dioxane was added portionwise. The suspension was stirred and maintained at pH 8.5–9.0 by adding NMM, during which **1a** gradually dissolved and TLC ($CHCl_3$/MeOH, 20:1) indicated complete disappearance of **1a**. The reaction mixture was evaporated under reduced pressure. The residue was dissolved in 30 mL of distilled water, and the solution was extracted with diethyl ether (3× 30 mL). The aqueous phase was acidified with saturated aqueous solution of $KHSO_4$ to pH 2 and extracted with EtOAc (3× 30 mL). The EtOAc phase was dried over anhydrous sodium sulfate, filtered and evaporated under reduced pressure to give 5.3 g (71%) of the title compound. Mp 151–152 °C; ^{1}H NMR (BHSC-300, DMSO-d_6) δ 12.85 (s, 2H), 8.29 (d, J = 6.9 Hz, 1H), 8.20 (d, J = 8.1 Hz, 1H), 6.90 (d, J = 8.1 Hz, 1H), 4.55 (t, J = 5.5 Hz, 2H), 4.24 (t, J = 4.5 Hz, 1H), 3.60 (s, 6H), 2.67 (m, 3H), 2.47 (m, 3H), 1.43 (s, 9H); ESI-MS (*m*/*z*) 492 $[M+H]^+$; $[\alpha]_D^{20}$15.1 (*c* 0.01, CH_3OH). Anal. Calcd for $C_{19}H_{29}N_3O_{12}$: C 46.44, H 5.95, N 8.55; found: C 46.63, H 5.83, N 8.75.

4.2.10. Boc-Asp[Asp(OMe)-Arg-OMe]-Asp(OMe)-Arg-OMe (8a). At 0 °C, 1-hydroxybenzotriazole (HOBT) (0.334 g, 2.48 mmol) and DCC (0.510 g, 2.48 mmol) were added to a solution of 0.578 g (1.18 mmol) of **7a** in 5 mL of anhydrous THF. The reaction mixture was stirred at 0 °C for 10 min and then 0.553 g (2.47 mmol) of HCl·H-Arg-OMe in 5 mL of anhydrous DMF was added. The reaction mixture was adjusted to pH 8–9 with NMM, stirred at 0 °C for 3 h and at room temperature for 12 h. The precipitated dicyclohexylurine (DCU) was removed by filtration and the filtrate was evaporated under reduced pressure. The residue was dissolved in 10 mL of distilled water and the solution was extracted with EtOAc (3× 30 mL). The aqueous phase was acidified with saturated aqueous solution of $KHSO_4$ to pH 2 and extracted with EtOAc (3× 30 mL). The aqueous phase was evaporated under reduced pressure and the residue was dissolved in 10 mL of anhydrous EtOH. After filtration and evaporation under reduced pressure the residue was purified by chromatography ($CHCl_3$/MeOH, 10:1) to give 0.784 g (80%) of the title compound. Mp 117–118 °C; ^{1}H NMR (BHSC-300, D_2O) δ 4.36 (t, J = 4.5 Hz, 2H), 4.34 (t, J = 3.6 Hz, 2H), 3.89 (t, J = 3.9 Hz, 1H), 3.68 (d, J = 7.8 Hz, 12H), 3.12 (t, J = 3.6 Hz, 4H), 2.80 (m, 3H), 2.71 (m, 3H), 1.78 (m, 4H), 1.50 (m, 4H), 1.31 (s, 9H); ESI-MS (*m*/*z*) 831$[M+H]^+$; $[\alpha]_D^{20}$ − 50.9 (*c* 0.01, CH_3OH). Anal. Calcd for $C_{33}H_{57}N_{11}O_{14}$: C 47.65, H 6.91, N 18.52; found: C 47.82, H 6.80, N 18.34.

4.2.11. Boc-Asp(Asp-Arg)-Asp-Arg (9a). Using the same procedure as that for **5a**, starting from 700 mg (0.842 mmol) of **8a**, 87 mg (90%) of the title compound was obtained as a colorless powder, which was used directly in the next reaction.

4.2.12. H-Asp(Asp-Arg)-Asp-Arg (10a). Using the same procedure as that for **3a**, starting from 587 mg (0.75 mmol) of **9a**, 358 mg (71%) of the title compound was obtained as a colorless powder. Mp 213–214 °C; IR (KBr) 3352, 2953, 2360, 1655, 1560, 1397, 1259, 752, 653 cm^{-1}; ^{1}H NMR (BHSC-300, D_2O) δ 4.48 (t, J = 4.5 Hz, 2H), 4.26 (t, J = 3.9 Hz, 1H), 4.12 (t,

J = 5.1 Hz, 2H), 3.09 (t, J = 6.6 Hz, 4H), 2.80 (m, 6H), 1.74 (t, J = 6.6 Hz, 4H), 1.64 (m, 4H); ESI-MS (*m*/*z*) 676 $[M+H]^+$; $[\alpha]_D^{20}$ − 14.0 (*c* 0.01, H_2O). Anal. Calcd for $C_{24}H_{41}N_{11}O_{12}$: C 42.66, H 6.12, N 22.80; found: C 42.49, H 6.01, N 22.99.

4.2.13. Cu(II)-Asp(Asp-Arg)-Asp-Arg [10a–Cu(II)]. Using the same procedure as that of **3a**–**Cu(II)**, starting from 124 mg (0.15 mmol) of **10a**, 34 mg (31%) of the title compound was obtained as blue powder. IR (KBr) 3351, 2964, 2401, 1635, 1396, 1193, 640 cm^{-1}; ESI-MS (*m*/*z*) 737$[M-1]^+$; $[\alpha]_D^{20}$ − 29.4 (*c* 0.01, H_2O). Anal. Calcd for $C_{24}H_{40}CuN_{11}O_{12}{\cdot}2H_2O$: C 37.23, H 5.73, N 19.90; found: C 37.06, H 5.61, N 19.73.

4.2.14. Boc-Glu(ONp)-ONp (1b). Using the same procedure as that for **1a**, starting from 5.0 g (0.02 mol) of Boc-Glu, 8.2 g (84%) of the title compound was obtained, which was used directly in the next reaction.

4.2.15. Boc-Glu(Arg)-Arg (2b). Using the same procedure as that for **2a**, starting from 1.8 g (3.68 mmol) of **1b** and 1.6 g (7.7 mmol) of HCl·H-Arg, 1.75 g (85%) of the title compound was obtained. Mp 89–91 °C; ^1H NMR (BHSC-300, D_2O) δ 4.15 (t, J = 4.2 Hz, 2H), 3.80 (t, J = 5.2 Hz, 1H), 3.08 (t, J = 7.35 Hz, 4H), 2.28 (t, J = 7.2 Hz, 2H), 1.98 (m, 2H), 1.80 (m, 4H), 1.64 (m, 4H), 1.32 (s, 9H); ESI-MS (*m*/*z*) 560 $[M+H]^+$; $[\alpha]_D^{20}$ − 22.7 (*c* 0.01, H_2O). Anal. Calcd for $C_{22}H_{41}N_9O_8$: C 47.22, H 7.38, N 22.53; found: C 47.03, H 7.27, N 22.33.

4.2.16. H-Glu(Arg)-Arg (3b). Using a similar procedure as that for **3a**, starting from 0.5 g (0.89 mmol) of **2b**, 319 mg (78%) of the title compound was obtained. Mp 140–142 °C; ^1H NMR (BHSC-300, D_2O) δ 4.22 (dd, J = 4.5, 9.0 Hz, 1H), 4.11 (dd, J = 3.9, 9.0 Hz, 1H), 3.74 (dd, J = 4.5, 11.1 Hz, 1H), 3.11 (dd, J = 5.7, 19 Hz, 4H), 2.37 (dd, J = 4.8, 14.7 Hz, 2H), 2.22 (m, 2H), 1.73 (m, 4H), 1.57 (m, 4H); ESI-MS (*m*/*z*) 460 $[M+H]^+$; $[\alpha]_D^{20}$ − 11.8 (*c* 0.01, H_2O). Anal. Calcd for $C_{17}H_{33}N_9O_6$: C 44.44, H 7.24, N 27.43; found: C 44.61, H 7.11, N 27.25.

4.2.17. Cu(II)-Glu(Arg)-Arg [3b–Cu(II)]. Using the same procedure as that for **3a**–**Cu(II)**, starting from 100 mg (0.218 mmol) of **3b**, 48 mg (42%) of the title compound was obtained. IR (KBr) 3367, 2966, 2360, 1596, 1411, 1207, 732 cm^{-1}; ESI-MS (*m*/*z*) 521 $[M-1]^+$; $[\alpha]_D^{20}$ + 43.4 (*c* 0.01, H_2O). Anal. Calcd for $C_{17}H_{32}CuN_9O_6{\cdot}2H_2O$: C 36.59, H 6.50, N 22.59; found: C 36.41, H 6.37, N 22.78.

4.2.18. Boc-Glu[Arg-Asp(OMe)-OMe]-Arg-Asp(OMe)-OMe (4b). Using the same procedure as that for **4a**, starting from 1.22 g (2.18 mmol) of **2b** and 902 mg (4.58 mmol) of H-Asp(OMe)-OMe, 1.2 g (65%) of the title compound was obtained. Mp 116–118 °C; ^1H NMR (BHSC-500, D_2O) δ 4.25 (t, J = 7.0 Hz, 2H), 4.01 (t, J = 5.2 Hz, 2H), 3.87(t, J = 7.35 Hz, 1H), 3.65 (d, J = 7.2 Hz, 12H), 3.11 (t, J = 4.5 Hz, 4H), 2.29 (m, 4H), 2.01 (m, 4H), 1.80 (m, 4H), 1.55 (m, 4H), 1.33 (s, 9H); ESI-MS (*m*/*z*) 846 $[M+H]^+$; $[\alpha]_D^{20}$ − 97.3 (*c* 0.01, CH_3OH). Anal. Calcd for: $C_{34}H_{59}N_{11}O_{14}$: C 48.28, H 7.03, N 18.21; found: C 48.11, H 7.16, N 18.38.

4.2.19. Boc-Glu(Arg-Asp)-Arg-Asp (5b). Using the same procedure as that for **5a**, starting from 500 mg (0.592 mmol) of **4b**, 319 mg (68%) of the title compound was obtained, which was used in the next reaction directly.

4.2.20. H-Glu(Arg-Asp)-Arg-Asp (6b). Using the same procedure as that for **3a**, starting from 300 mg (0.380 mmol) of **5b**, 180 mg (69%) of the title compound was obtained. Mp 161–163 °C; IR (KBr) 3346, 2879, 2360, 1652, 1589, 1386, 1259, 748, 669 cm^{-1}; ^1H NMR (BHSC-500, D_2O) δ 4.65 (dd, J = 5.0, 10.0 Hz, 2H), 4.35 (t, J = 7.5 Hz, 1H), 4.23 (dd, J = 6, 8 Hz, 1H), 3.85 (dd, J = 5.0, 8.5 Hz, 1H), 3.11 (t, J = 6.5 Hz, 4H), 2.86 (m, J = 5.0 Hz, 4H), 2.37(t, J = 7.0 Hz, 1H), 2.28 (dd, J = 8.0, 16.0 Hz, 1H), 2.12 (t, J = 8.0 Hz, 1H) 2.00 (t, J = 6.5 Hz, 1H), 1.76 (m, J = 8.0, 14.5 Hz, 2H), 1.70–1.62 (m, 2H), 1.57 (m, J = 6.5, 16.5 Hz, 4H); ESI-MS (*m*/*z*) 690 $[M+H]^+$; $[\alpha]_D^{20}$ − 22.6 (*c* 0.01, H_2O). Anal. Calcd for $C_{25}H_{43}N_{11}O_{12}$: C 43.54, H 6.28, N 22.34; found: C 43.36, H 6.16, N 22.50.

4.2.21. Cu(II)-Glu(Arg-Asp)-Arg-Asp [6b-Cu(II)]. Using the same procedure as that for **3a**–**Cu(II)**, starting from 0.100 g (0.145 mmol) of **6b**, 40 mg (37%) of the title compound was obtained as blue powder. ESI-MS (*m*/*z*) 750 $[M-1]^+$; $[\alpha]_D^{20}$ − 8.8 (*c* 0.01, H_2O). Anal. Calcd for $C_{25}H_{42}CuN_{11}O_{12}{\cdot}2H_2O$: C 38.09, H 5.88, N 19.55; found: C 38.26, H 5.75, N 19.70.

4.2.22. Boc-Glu[Asp(OMe)]-Asp(OMe) (7b). Using the same procedure as that for **7a**, starting from 5.0 g (0.01 mol) of **1b** and 3.84 g (0.02 mmol) of HCl·H-Asp(OCH_3), 4.1 g (81%) of the title compound was obtained. Mp 83–85 °C; ^1H NMR (BHSC-300, DMSO-d_6) δ 12.85 (s, 2H), 8.16 (d, J = 8.1 Hz, 1H), 8.12 (d, J = 8.1 Hz, 1H), 6.92(d, J = 8.1 Hz, 1H), 4.55 (t, J = 5.2 Hz, 2H), 3.88 (t, J = 7.0 Hz, 1H), 3.59 (s, 6H), 2.70 (m, 4H), 2.19 (m, 2H), 1.72 (m, J = 6.5 Hz, 2H), 1.43 (s, 9H); ESI-MS (*m*/*z*) 506 $[M+H]^+$; $[\alpha]_D^{20}$3.2 (*c* 0.01, CH_3OH). Anal. Calcd for $C_{20}H_{31}N_3O_{12}$: C 47.52, H 6.18, N 8.31; found: C 47.67, H 6.06, N 8.50.

4.2.23. Boc-Glu[Asp(OMe)-Arg-OMe]-Asp(OMe)-Arg-OMe (8b). Using the same procedure as that for **8a**, starting from 4.0 g (0.008 mol) of **7b** and 3.8 g (0.017 mmol) of HCl·H-Arg-OCH_3, 4.68 g (70%) of the title compound was obtained. Mp 118–119 °C; ^1H NMR (BHSC-500, D_2O) δ 4.38 (t, J = 5.2 Hz, 2H), 4.14 (t, J = 5.2 Hz, 2H), 3.91 (t, J = 7.35 Hz, 1H), 3.62 (s, J = 7.2 Hz, 12H), 3.10 (t, J = 6.5 Hz, 4H), 2.85 (m, J = 6.5 Hz, 2H), 2.78 (m, J = 6.4 Hz, 2H), 2.29 (d, J = 6.4 Hz, 2H), 2.04 (m, 2H), 1.78 (m, 4H), 1.52 (m, 4H), 1.31 (s, 9H); ESI-MS (*m*/*z*) 846 $[M+H]^+$; $[\alpha]_D^{20}$ − 30.3 (*c* 0.01, CH_3OH). Anal. Calcd for $C_{34}H_{59}N_{11}O_{14}$: C 48.28, H 7.03, N 18.21; found: C 48.11, H 7.13, N 18.40.

4.2.24. Boc-Glu(Asp-Arg)-Asp-Arg (9b). Using the same procedure as that for **5a**, starting from 0.239 g (0.282 mmol) of **8b**, 200 mg (90%) of the title compound was obtained, which was used directly in the next reaction.

4.2.25. H-Glu(Asp-Arg)-Asp-Arg (10b). Using the same procedure as that for **3a**, starting from 200 mg (0.253 mmol) of **9b**, 150 mg (86%) of the title compound was obtained. Mp 147–149 °C; IR (KBr) 3349, 2952, 2360, 1652, 1558, 1394, 1253, 752, 611 cm^{-1}; ^1H NMR (BHSC-500, D_2O) δ 4.49 (t, $J = 4.0$ Hz, 2H), 4.14 (t, $J = 4.5$ Hz, 2H), 4.11 (t, $J = 4.5$ Hz, 1H), 3.07 (t, $J = 6.5$ Hz, 4H), 2.68 (dd, $J = 9.0$ Hz, $J = 14.5$ Hz, 4H), 2.08 (m, 4H), 1.75 (m, 4H), 1.50 (m, $J = 4.5$ Hz, 4H); ESI-MS (*m*/*z*) 690 $[M+H]^+$; $[\alpha]_D^{20} - 11.5$ (*c* 0.01, H_2O). Anal. Calcd for $C_{25}H_{43}N_{11}O_{12}$: C 43.54, H 6.28, N 22.34; found: C 43.40, H 6.21, N 22.52.

4.2.26. Cu(II)-Glu(Asp-Arg)-Asp-Arg [10b–Cu(II)]. Using the same procedure as that for **3a**–**Cu(II)**, starting from 100 mg (0.145 mmol) of **10b**, 26 mg (23%) of the title compound was obtained. IR (KBr) 3350, 2965, 2340, 1589, 1397, 1186, 779 cm^{-1}; ESI-MS (*m*/*z*) 750 $[M-1]^+$; $[\alpha]_D^{20} - 40.7$ (*c* 0.01, H_2O). Anal. Calcd for $C_{25}H_{42}CuN_{11}O_{12}\cdot 2H_2O$: C 38.09, H 5.88, N 19.55; found: C 38.25, H 5.74, N 19.37.

4.3. In vitro anti-platelet aggregation assay

An H-10 cell counter was used to determine the platelet count. A two-channel Chronolog aggregometer was used to evaluate platelet aggregation. After collection, pig blood was centrifuged at 100*g* for 10 min and the platelet-rich plasma (PRP) was removed. The remaining blood was centrifuged for a further 10 min at 1500g to prepare platelet-poor plasma (PPP). The final platelet count of the citrated plasma samples was adjusted to 2×10^8 platelets/mL with autologous PPP. In the assays 0.5 mL of the adjusted plasma sample and 5 μL of NS or a solution of (**3,6,10)a,b** (in a range of concentrations from 10^{-2} to 10^{-4} M) or [**(3,6,10)a,b**]–**Cu(II)** in NS (10^{-2} M to 10^{-4} M) was added to the testing tube. After adjustment of the baseline, 5 μL of a solution of platelet-activating factor in NS (PAF, final concentration 10^{-7} M), or 5 μL of a solution of adenosine diphosphate in NS (ADP, final concentration 10^{-5} M), or 5 μL of a solution of arachidonic acid in NS (AA, final concentration 3.5×10^{-4} M), or 5 μL of a solution of thrombin in NS (TH, final concentration 0.2 U/mL) was then added to the testing tube. The testing tube was stirred at 37 °C for 5 min allowing the platelets having a maximal aggregation, while the aggregometer automatically recorded the aggregation curve. The peak height of this aggregation curve was defined as the maximal aggregation rate (Am). The inhibition effect of (**3,6,10)a,b** and [**(3,6,10)a,b**]–**Cu** on PAF-, ADP-, AA-, or TH-induced platelet aggregation was represented by the difference between the Am of NS and that of (**3,6,10)a,b**or [**(3,6,10)a**, **b**]–**Cu**, the aggregation inhibition rate was calculated by Inhibition = [(Am of NS) − (Am of (**3,6,10) a,b**or [(**3,6,10) a,b**]–**Cu(II)**) ÷ (Am of NS), and the IC_{50} value was determined via the program GWBASIC.EXE.

4.4. In vivo anti-thrombosis activity in rat model

The assessments described herein were performed based on a protocol reviewed and approved by the ethics committee of Capital Medical University. The committee assures that the welfare of the animals was maintained in accordance to the requirements of the animal welfare act and according to the guide for care and use of laboratory animals.

4.4.1. Intravenous administration of (3,6,10)a,b and [(3,6,10)a,b]–Cu(II). Aspirin, (**3,6,10) a,b**, and [**(3,6,10) a,b**]–**Cu(II)** were dissolved in NS just before use and kept in an ice bath. Male Wistar rats weighing 250–300 g (purchased from Animal Center of Peking University) were used, and the method of Ji et al.[28] was followed. Venom-derived fractions were dissolved in NS just before use and kept in an ice bath. The rats were anesthetized with pentobarbital sodium (80.0 mg/kg, ip), and the right carotid artery and left jugular vein were separated. A weighed 6 cm thread was inserted into the middle of a polyethylene tube. The polyethylene tube was filled with heparin sodium (50 IU/mL in NS) and one end was inserted into the left jugular vein. From the other end of the polyethylene tube, heparin sodium was injected as anticoagulant, then NS or (**3,6,10) a,b** or [**(3, 6, 10)a,b**]–**Cu(II)** were injected, and this end was inserted into the right carotid artery. Blood flowed from the right carotid artery to the left jugular vein through the polyethylene tube for 15 min. The thread was recovered to obtain the thrombus weight.

4.4.2. Oral administration of 10a. Solutions of aspirin or **10a** in NS were given orally to male Wistar rats (weighing 250–300 g, purchased from Animal Center of Peking University). Then the rats were anesthetized with pentobarbital sodium (80.0 mg/kg, ip). Thirty min later, the right carotid artery and left jugular vein of the rat were separated. A weighed 6 cm thread was inserted into the middle of a polyethylene tube. The polyethylene tube was filled with heparin sodium (50 IU/mL in NS) and one end was inserted into the left jugular vein and the other end was inserted into the right carotid artery. Blood flowed from the right carotid artery to the left jugular vein through the polyethylene tube for 15 min. The thread was removed and weighed, and the weight of the wet thrombus was recorded.

4.5. Particle size and zeta-potential tests of (3,6,10)a,b and [(3,6,10)a,b]–Cu(II)

The size of the nano-particles of (**3,6,10)a,b** and [**(3,6,10) a,b**]–**Cu(II)** assembled in NS was analyzed using a Malvern's Zeta Sizer (Nano-ZS90) with DTS (Nano) Program. In the determination, 1 mg each of (**3,6,10) a,b** or [**(3,6,10)a,b**]–**Cu(II)** was dissolved in 1 mL of normal saline (NS, 0.9% NaCl aqueous solution, pH 7.3–7.4) to prepare the testing solution (1 mg/mL, pH 6.8–7.1). This stock solution was kept in a 4 °C refrigerator before use. In the test, the system temperature was 25 °C, the data collection time was 50 s and total collection 5 min. The Sizer automatically read the mean size, half-peak width and % intensity of the peak.

Zeta-potentials of the nano-particles assembled from (**3**,**6**, **10)a, b** and [**(3,6,10)a,b**]–**Cu(II)** in NS were analyzed using a ZetaPlus Potential Analyzer (ZetaPlus S/N 21394, Brookhaven Instruments Coorporation) with

BIC Zeta Potential Analyzer. The concentration of the solution of (**3,6,10**)**a,b** and [(**3, 6, 10**)**a,b**]–**Cu(II)** in NS was 1 mg/mL and the testing temperature was 25 °C.

4.6. UV and CD spectral tests of (3,6,10)a,b and [(3,6,10)a,b]–Cu[12]

Electronic absorption spectra (UV–vis) of (**3,6,10**) **a,b** (pH 4.7, 3.8, 3.7, 4.1, 4.4 and 3.6, aqueous solution, 1 mM, 25 °C) and [(**3,6,10**) **a,b**]–**Cu(II)** (pH 6.3, 6.0, 5.5, 4.5, 5.3 and 5.2, aqueous solution, 1 mM, 25 °C) were recorded with a UV–visible spectrophotometer (UV-2550, Shimadzu). Circular dichroism (CD) spectra of **(3,6,10)a,b** (pH 4.7, 3.8, 3.7, 4.1, 4.4 and 3.6, aqueous solution, 1 mM, 25 °C) and [**(3,6,10)a,b**]–**Cu(II)** (6.3, 6.0, 5.5, 4.5, 5.3 and 5.2, aqueous solution, 1 mM, 25 °C) were obtained on a spectropolarimeter with JASCO Canvas Program (Model J-810, Jasco, Japan) over a range of 200–750 nm.

4.7. Nano-size particle tests of (3,6,10)a,b and [(3,6,10)a,b]–Cu powders

Solutions of (**3,6,10**)**a,b** and [(**3,6,10**)**a,b**]–**Cu** in double distilled water (1 mg/mL) were evaporated at room temperature to provide dry powder. The particle size of the powders of (**3,6,10**)**a,b** and [(**3,6,10**)**a,b**]–**Cu** were measured by transmission electron microscopy (TEM, Model JEM-1230, JEOL, Japan). Their morphologies were illustrated by photographs, and particle sizes represented by diameters.

Acknowledgments

This work was supported by Beijing Area Major Laboratory of Peptide and Small Molecular Drugs, the 973 Project of China (2006CB708501) and Natural Scientific Foundation of China (30472071).

References and notes

1. Fitzgerald, D. J.; Roy, L.; Catella, F.; Fitzgerald, G. A. *N. Engl. J. Med.* **1986**, *315*, 983–989.
2. Fuster, V.; Chesebro, J. H. *N. Engl. J. Med.* **1986**, *315*, 1023–1025.
3. Willerson, J. T.; Hillis, L. D.; Winniford, M.; Buja, L. M. *J. Am. Coll. Cardiol.* **1986**, *8*, 245–251.
4. Packham, M. A. *Can. J. Physiol. Pharmacol.* **1994**, *72*, 278–284.
5. Stein, B. S.; Fuster, V.; Israel, D. M.; Cohen, M.; Badimon, L.; Badimon, J.; Chesebro, J. H. *J. Amer. Coll. Cardiol.* **1989**, *14*, 813–836.
6. Stein, B.; Fuster, V. *Cardiovasc. Drugs Ther.* **1989**, *3*, 797–813.
7. Furchgott, R. F.; Zawadzki, J. V. *Nature (London)* **1980**, *288*, 373–376.
8. Moncada, S. R.; Palmer, M. J.; Higgs, E. A. *Pharmacol. Res.* **1991**, *43*, 109–142.
9. Murad, F. *J. Clin. Invest.* **1986**, *78*, 1–5.
10. Salvemini, D.; Radziszewski, W.; Korbut, R.; Vane, J. *Br. J. Pharmacol.* **1990**, *101*, 991–995.
11. Feelisch, M. *J. Cardiovasc. Pharmacol.* **1991**, *17*, 25–33.
12. George, G.; Costas, T.; Dimitris, T.; Christodoulos, S.; Pavlos, T. *Atherosclerosis* **2001**, *154*, 255–267.
13. Tang, Z.; Wang, Y.; Xiao, Y.; Zhao, M.; Peng, S. *Thrombosis Res.* **2003**, *110*, 127–133.
14. Wang, Y. Y.; Tang, Z. Y.; Dong, M.; Liu, X. Y.; Peng, S. Q. *Acta Pharmacol. Sin.* **2004**, *25*, 469–473.
15. Reches, M.; Gazit, E. *Curr. Nanosci.* **2006**, *2*, 105–111.
16. Zanuy, D.; Nussinov, R.; Aleman, C. *Phys. Biol.* **2006**, *3*, S80–S90.
17. Scheibel, T. *Curr. Opin. Biotechnol.* **2005**, *16*, 423–427.
18. Gao, X.; Matsui, H. *Adv. Mater.* **2005**, *17*, 2037–2050.
19. Zhao, X.; Zhang, S. *Trends Biotechnol.* **2004**, *22*, 470–476.
20. Rajagopal, K.; Schneider, J. P. *Curr. Opin. Struct. Biol.* **2004**, *14*, 480–486.
21. Montet, X.; Funovics, M.; Montet-Abou, K.; Weissleder, R.; Lee, J. *J. Med. Chem.* **2006**, *49*, 6087–6093.
22. Carny, O.; Shalev, D.; Gazit, E. *Nano Lett.* **2006**, *6*, 1594–1597.
23. Sarikaya, M.; Tamerler, C.; Jen, A. K. Y.; Schulten, K.; Baneyx, F. *Nat. Mater.* **2003**, *2*, 577–585.
24. Patolsky, F.; Weizmann, Y.; Willner, I. *Nat. Mater.* **2004**, *3*, 692–695.
25. Ghosh, S.; Verma, S. *Tetrahedron Lett.* **2007**, *48*, 2189–2192.
26. Banerjee, A. I.; Yu, L.; Matsui, H. *Proc. Natl. Acad. Sci. U.S.A.* **2003**, *100*, 14678.
27. Casolaro, M.; Chelli, M.; Ginanneschi, M.; Laschi, F.; Muniz-Miranda, M.; Papini, A. M.; Sbrana, G. *Spectrochim. Acta Part A* **1999**, *55*, 1675–1689.
28. Łodyga-Chruscinska, E.; Ołdziej, S.; Micera, G.; Sanna, D.; Chruscinski, L.; Olczak, J.; Zabrocki, J. *J. Inorg. Biochem.* **2004**, *98*, 447–458.